Eur. Phys. J. D **33**, 335–342 (2005)
DOI: 10.1140/epjd/e2005-00069-9

THE EUROPEAN PHYSICAL JOURNAL D

The electron affinities of O, Si, and S revisited with the photodetachment microscope

C. Blondel[a], W. Chaibi, C. Delsart, C. Drag, F. Goldfarb[b], and S. Kröger[c]

Laboratoire Aimé-Cotton[d], Centre national de la recherche scientifique, bâtiment 505, 91405 Orsay Cedex, France

Received 31 January 2005 / Received in final form 30 March 2005
Published online 12 May 2005 –

Abstract. Photodetachment microscopy has been performed on a beam of $^{32}S^-$ ions. Analysing the electron images obtained, we find that the electron affinity measurements performed with the photodetachment microscope contain a small bias, due to the difference between the actual and assumed values of the applied electric field. Having a measure of this bias, we can reanalyse older data recorded on the negative ions O^- and Si^- along similar lines. As a consequence, the values of the electron affinities of Oxygen, Silicon and Sulfur can be given with an improved accuracy. The recommended values (with expanded uncertainties) are now 11 784.676(7) cm^{-1} for ^{16}O, 11 207.246(8) cm^{-1} for ^{28}Si, and 16 752.974(5) cm^{-1} for ^{32}S, i.e. 1.461 113 5(12), 1.389 521 3(13) and 2.077 104 0(9) eV, respectively.

PACS. 32.80.Gc Photodetachment of atomic negative ions – 03.75.-b Matter waves – 07.78.+s Electron, positron, and ion microscopes; electron diffractometers – 32.10.Hq Ionization potentials, electron affinities

1 Measuring electron affinities with the photodetachment microscope

1.1 Photodetachment microscopy

Photodetachment of a negative ion may be described as one of the most simple processes in atomic physics. Absorption of a photon brings one electron into a structureless detachment continuum. Interaction of this electron with the residual neutral is so weak that the continuum state can be described, in a very good approximation, as a free spherical wave. Photodetachment provides the experimentalist with nearly perfect pointlike free-electron sources.

When an electron is emitted from such a source set in a homogeneous external electric field, its trajectories become parabolas. As a well-known theorem in ballistics, at a fixed initial energy only no or two parabolas can reach a given detection point. An electron interference phenomenon may thus occur, which will give rise to ringlike fringe patterns. Such interference patterns were observed for the first time from the negative ion Br^- in 1996, following a suggestion dating back to 1981 [1]. This was the birth of 'photodetachment microscopy' [2].

Having an interference pattern instead of an electron spot as the output of a photodetachment process makes it possible to measure the photoelectron energy ϵ with interferometric accuracy. Uncertainties down to 1 μeV can be reached [3] by fitting the obtained electron images with what is expected from the propagation from a pointlike source in a uniform acceleration field [4]. Subtracting the electron energy ϵ from the energy of the absorbed photon $h\nu$, one can find the electron affinity ${}^eA$ of the species with a similar accuracy [5]:

$$ {}^eA = h\nu - \epsilon. \tag{1}$$

1.2 Doppler effect

A difficulty encountered when implementing the above method is that the photon energy seen by the ion is not the same as the one measured in the laboratory. Whatever the settings, the exact angle at which the laser and ion beam intersect cannot be known with a very good accuracy. To circumvent this difficulty, a double-pass scheme is used, in which the laser illuminates the ion beam twice, in counterpropagating directions. A scheme of the experimental set-up used for that purpose is shown in Figure 1.

Since photodetachment at the first laser crossing is far from being saturated, two distinct electron spots are produced from the same ion beam. An example of such a pair of spots is shown in Figure 2. Their fitting to the theoretical formula yields two photoelectron energies ϵ and ϵ'.

[a] e-mail: christophe.blondel@lac.u-psud.fr
[b] *Present address*: Institut für Experimentalphysik, Universität Wien, Boltzmanngasse 5, 1090 Wien, Austria.
[c] *Present address*: Institut für Atomare und Analytische Physik, Technische Universität Berlin, Hardenbergstr. 36, 10623 Berlin, Germany.
[d] URL: http://www.lac.u-psud.fr

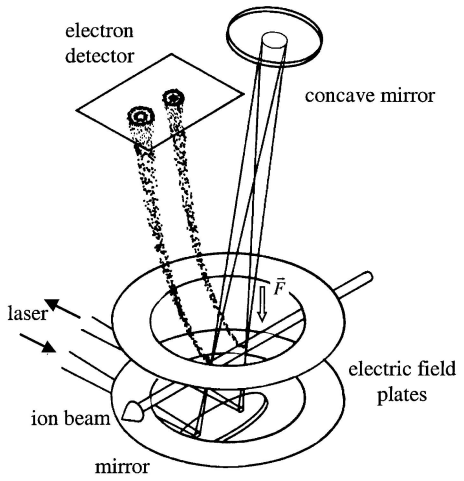

Fig. 1. Scheme of the double-pass photodetachment set-up. A concave mirror is used to focus the laser back onto the ion beam. For the sake of making all parts of the set-up visible, only two of the 28 parallel plates used to produce the electric field are represented, and the drawing is not made to scale.

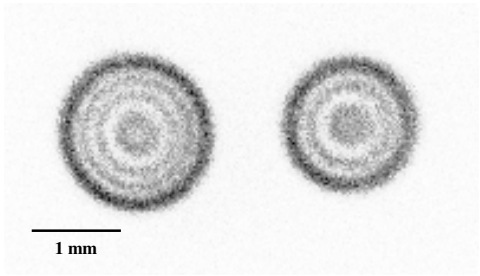

Fig. 2. A pair of detachment interference patterns obtained from S^- detached in an electric field $F = 258$ V/m at the wavelength $\lambda \simeq 596\,885$ pm (vacuum). Fitting the theory to the experimental image one finds that the electrons in the left and right spots have been emitted with kinetic energies $\epsilon \simeq 0.713$ and $\epsilon' \simeq 0.562\,\mathrm{cm}^{-1}$ respectively.

If one of the spots results from photodetachment by positively Doppler-shifted photons, the other one is produced by symmetrically negatively Doppler-shifted photons. Replacing ϵ by the average $(\epsilon + \epsilon')/2$ makes a first-order correction of the unknown Doppler-effect.

The second-order Doppler correction multiplies the photon energy by the same $\gamma = \left[1 - \beta^2\right]^{-\frac{1}{2}}$ factor, with $\beta = v/c$, for all directions of illumination. Additional corrections due to the fact that the two laser beams are not exactly anti-parallel and that the ion beam undergoes some deflection by the electric field between the two interaction zones can be written as corrections to the photon energy too. Writing

$$\nu' = \gamma \left[1 \pm \beta \frac{D}{2} \left(\frac{1}{R} - \frac{F}{2U}\right)\right] \nu \qquad (2)$$

with D the distance between the electron spots, R the radius of curvature of the mirror, and U the acceleration voltage of the ion beam, one can write finally [3]

$${}^eA = h\nu' - \frac{1}{2}(\epsilon + \epsilon'). \qquad (3)$$

The $\pm$ sign in equation (2) corresponds to making the reflected laser illuminate the ion beam either upstream or downstream of the first illumination zone. The factor linking ν' to ν can be calculated with an error smaller than ± 0.7 mk ($1\,\mathrm{mk} \equiv 10^{-3}\,\mathrm{cm}^{-1}$).

1.3 Total uncertainty with no field correction

The total expanded uncertainty of the electron affinities measured with the photodetachment microscope so far [3,5,6] has been calculated as the sum of twice the standard deviation of $\langle {}^eA \rangle$, as given by averaging a large number of measurements, and the possible systematic error that cannot be reduced by averaging. The ± 0.7 mk uncertainty on the ν'/ν ratio is a part of the latter. The possible systematic error made when measuring ν also comes in, for about ± 2 mk or ± 0.8 mk, depending on the kind of lambdameter used (see below). Last but not least, a systematic uncertainty on the measured energies ϵ and ϵ' arises from the fact that measuring the phase of the interferograms, one only measures the $\epsilon^{3/2}/F$ ratio [6], with F the applied electric field. A $\pm 1.2\%$ uncertainty on the intensity of the applied electric field thus produces a $\pm 0.8\%$ uncertainty on the ϵ and ϵ' values used in formula (3). Since the mean energy reached above threshold is between 0.4 and $1.2\,\mathrm{cm}^{-1}$, this contribution is roughly ± 7 mk on the final electron affinity.

1.4 Beyond the electric field uncertainty

In principle, the existence of a relative bias on the $(\epsilon + \epsilon')/2 = \overline{\epsilon}$ term can be taken into account by extrapolating the measured ${}^eA(\overline{\epsilon})$ values down to ${}^eA(0)$. Unfortunately, we cannot make $\overline{\epsilon}$ arbitrarily small in the experiment, because a minimum energy is required to make the image a real fringe pattern and not a trivial electron spot. As can be observed in Figure 3, which displays only one of the ten experimental series recorded on S^-, the vertical dispersion of the experimental ${}^eA(\overline{\epsilon})$ measurements consequently brings in a lot of uncertainty on the ${}^eA(0)$ extrapolated value.

The trend for a slightly positive derivative of the measured electron affinity as a function of $\overline{\epsilon}$ has nevertheless been confirmed by a majority of experimental series. Its average value is about 0.012, which reveals a systematic overestimation of ${}^eA$ by 1.2% of $\overline{\epsilon}$. This, in turn, can be attributed to an underestimation of ϵ and ϵ' by the same amount. As perturbations of the interference phase would likely not result in so constant an effect (rescattering would rather produce phase-dependent perturbations), a tentative interpretation is that the electric field has been underestimated by as much as 1.8%. A possible explanation for that underestimation will be given below.

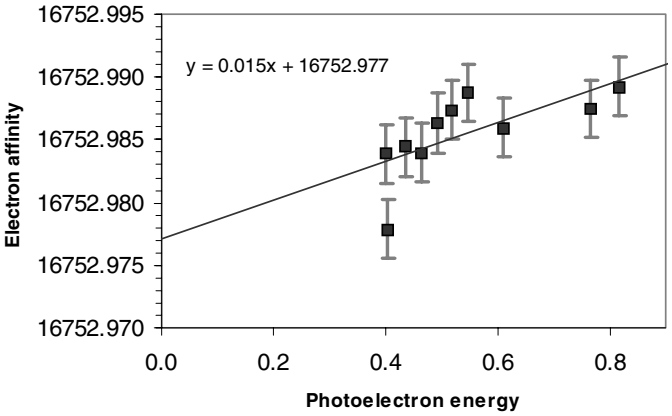

Fig. 3. Electron affinity as a function of the mean kinetic energy of the photoelectron (units are cm^{-1} for both), for a series of detachment experiments on S^-, in an electric field $F \simeq 260\,V/m$, assuming the presence of a magnetic field $B_\perp = 8 \times 10^{-8}$ T. The adjusted slope K in this case is $1.5 \pm 0.5\%$.

The aim of the present work is to revisit the ancient data recorded on O^- and Si^-, together with new experimental data just obtained on S^-, and apply this new 'F-correction' method so as to give a better determination of the electron affinities of oxygen, silicon and sulfur.

1.5 Error fluctuations

If the relative error on the electric field was a constant one, the slope K of the $\overline{\epsilon}$ correction, which cannot be determined very precisely on a single experimental series, could be made the object of a two-dimensional averaging procedure with the electron affinity ${}^eA$ itself. Unfortunately, because the place where the ions interact with the laser beam is not exactly fixed in the interaction chamber, the relative error made on the electric field may itself vary from one series to the other one. K is thus not a unique variable and two-dimensional (K,${}^eA$) correlated averaging does not apply. On the other hand, even though the electric field error varies from place to place, it necessarily has a limited dispersion. This suggests to improve the accuracy on the extrapolated ${}^eA(\overline{\epsilon} = 0)$ values by constraining the linear regressions to have slopes K not too different from the mean value $\langle K \rangle$. Following this idea, after having made a free-K linear regression of all series, we shall calculate the mean value of the obtained slopes and constrain the K values, making linear regressions again, with a finite standard deviation σ_K around $\langle K \rangle$. The overall averaged value of ${}^eA$ will be calculated with different hypotheses for this standard deviation and the dispersion will be used to estimate the final uncertainty. The way to actually impose a standard deviation on the slope of a linear regression is described in Appendix A.

1.6 Magnetic field correction

A hypothesis can also be made about the existence of a residual magnetic field in the interaction zone. Magnetic shielding by a double layer of μ-metal is supposed to make the residual magnetic field smaller than 0.5 μT in the interaction region. The possible presence of a transverse component of the order of 10^{-7} T must be taken into account in the quantitative analysis.

The effect of a longitudinal magnetic field is expected to reduce the radius of the interferograms by magnetic focusing, with no change of the number of rings, i.e. of the phase used for the measurement [7]. The effect of a transverse magnetic field $B_\perp$ can be calculated by considering the experiment from the reference frame that makes the electromagnetic field a pure electric field F', or (if the $B_\parallel$ component is not zero), from the reference frame that makes $\boldsymbol{F}'$ and $\boldsymbol{B}'$ parallel. As the density of presence probability of the electron, i.e. the structure and number of rings in the interference pattern, is a relativistic invariant, it will be determined, even in the laboratory frame, by the value of $|F'|$. At the lowest order in $cB_\perp/F$,

$$F' = \sqrt{F^2 - c^2 B_\perp^2}. \tag{4}$$

This correction is always an F-lowering one. In other words, it tells that the effective electric field may be lower than what we have assumed, hence that we have overestimated the electron energies. It cannot thus be used to explain the positive slope observed in the data, such as the ones of Figure 3. The magnetic field effect is an additional one, the clear demonstration of which would require varying the electric field on more than one order of magnitude (which could not be done). We have dealt with this possible effect by trying several different possible values of $B_\perp$ to correct the measured ϵ values, within realistic limits. The resulting variation of the measured electron affinity ${}^eA(0)$ gives one more contribution to the final uncertainty. The numerical values for this variation will be given for every studied atom below.

2 Experimental set-up for S^- detachment

2.1 Ion beam

The O^- and Si^- detachment experiments have been described elsewhere [3,5,6]. S^- ions can be produced from the same hot cathode discharge source, fed with a commercial mixture of 2% CS_2 and 98% Ar. The source is set at a potential of –1200 V with respect to the (grounded) extraction electrode. Mass 32 is selected by a Wien velocity filter. Electrostatic optics is used to collimate the beam. A quadrupolar deflector eliminates the neutral particles produced in the first chambers, where the residual pressure is higher. An electrostatic decelerator finally reduces the ion kinetic energy down to either 300 or 400 eV just before the photodetachment zone. The ion beam intensity in the interaction region is typically 200 pA.

2.2 Origin of the electric field bias

Interaction of the ion beam with the detaching laser takes place in a uniform electric field region shielded against the

Earth magnetic field by a double layer of μ-metal. The electric uniform field is produced by a set of 28 parallel stainless steel plates, with an open central zone of 27 mm in diameter. The plates around the interaction zone are 14 mm apart.

Deviations of the electric field intensity from its nominal value can have several causes. The first one is the accuracy of the potentials set on the plates (essentially the two plates that surround the interaction zone). The voltage generators and divisors used have a 10^{-3} accuracy. The second source of possible deviation is the real distance set between the plates, which cannot be guaranteed to be more accurate than $\pm 1\%$ of the supposed 14 mm. Moreover the thickness of the plates alone, even though their central opening is larger than the 14 mm spacing, has the effect of increasing the field by nearly 0.4 % on axis. Finally the displacement of the interaction zone from the symmetry centre of the electrostatic plates system can play a role both in the deviation and in the dispersion of the real field intensity. Calculations with SIMION [8] show that a longitudinal displacement of 4 mm, which is about the distance by which the ion beam is bent by the electric field, is enough to produce a 10^{-3} relative variation.

2.3 Laser excitation

Photodetachment of S^- has been studied either from the ground $^2P_{3/2}$ level of the negative ion to the ground $^3P_2$ level of S near 596.9 nm, or from the fine-structure excited level $^2P_{1/2}$ of the ion to either the $^3P_2$ or $^3P_1$ levels of the neutral, near 614.6 and 600.0 nm, respectively (wavelengths are given in vacuum). Photo-excitation is provided by a single mode CW dye laser (Spectra-Physics 360 A) pumped by an argon-ion laser. We operate with Rhodamine 590 in 5% methanol and 95% ethylene-glycol. The power of the laser is typically 400 mW, for a pump power of about 5 W.

Short-time stabilisation is obtained by servo-locking the CW dye laser frequency on a static sigmameter [9]. For the long time stabilization, the sigmameter itself has its optical path difference servo-locked with a dual-polarization stabilized He–Ne laser. The whole stabilization system makes the laser stability better than 10 MHz during the whole acquisition time (typically 20 minutes).

The wavelength is measured either by comparison to the wavelength of an I_2 saturated absorption stabilized He-Ne laser in a Michelson interferometer [10,11] or by measurement in an *Ångstrom* WS-8 lambdameter. The accuracy of the wavenumber so measured is ± 2 mk or ± 0.8 mk respectively.

2.4 Electron detection

The electron detector [12] of photodetached electrons is based on a stack of five microchannel plates (MCPs) followed by a resistive-anode position encoder. Each detected electron has its arrival position measured and recorded in a two-dimensional histogram. After a few million electrons have been recorded (which takes 1000 s typically), the two-dimensional histogram becomes a good approximation of the square modulus of the electron continuum wavefunction, i.e. the interferogram to be analysed.

3 Sulfur

3.1 History of the electron affinity measurements of S

The total photodetachment cross-section of a negative ion set in an electric field exhibits oscillations that reveal the existence of the interference brought to observation by the photodetachment microscope. S^- may be the ion on which this oscillation received the greatest experimental [13–15] and theoretical [16] attention. In addition, $^{33}S^-$ is one of the rare examples of a negative ion the hyperfine structure of which has been actually measured [17]. The use of a Penning trap made it possible to study S^- photodetachment towards the excited ^1D term [18], photodetachment in a magnetic field [19–21] and in parallel electric and magnetic fields [22].

As a remarkable achievement of one of the first laser photodetachment studies [23], the electron affinity of sulfur was already known to the fourth significant digit in 1970, as ${}^eA(S) = 2.0772 \pm 0.0005$ eV, i.e. $16\,754(4)\,cm^{-1}$. That was, at the time, the best known of all electron affinities. In 1985, photodetachment near threshold in the presence of a magnetic field [21] led, by extrapolation to the zero-field threshold, to ${}^eA(S) = 16\,752.967(29)\,cm^{-1}$. The corresponding data were merged with an unpublished result, quoted in reference [21] to be ${}^eA(S) = 16\,752.966(10)\,cm^{-1}$, to produce the last admitted value, ${}^eA(S) = 16\,752.966(8)\,cm^{-1}$ [24].

3.2 Results

Ten series of double detachment interferograms similar to the one presented in Figure 2 have been recorded, making a total of 109 images. For each series, recorded with fixed acceleration and ion beam settings, a linear regression such as the one presented in Figure 3 can be made, to yield an 'F-corrected' measurement. Before the regression is made, every individual ϵ and ϵ' value is corrected for the possible presence of a transverse magnetic field $B_\perp$. For the statistical treatment, the uncertainty associated with every ϵ value is the sum of the statistical fitting uncertainty and of the maximum error of the laser wavelength measurement.

For a magnetic field $0 \leq B_\perp \leq 6 \times 10^{-8}$ T, the average dependence of the measured ${}^eA$ on $\overline{\epsilon}$ has a slope K between 1.3 and 1.7%. Table 1 shows the results obtained with no constraint and with the additional hypothesis that the K distribution obeys a normal law with an assumed 0.6% or 0.3% standard deviation. It also shows the ${}^eA(S)$ values obtained with different hypotheses for the transverse magnetic field $B_\perp$. An idea of the most likely value of the magnetic field can be given by watching either the residual dispersion of the individually measured electron affinities with respect to the linear fitting curve such as the one drawn in Figure 3, or by the effective dispersion

Table 1. Possible values for the electron affinity of sulfur (cm^{-1}), depending on the deviation admitted for the energy bias and the assumed value of the residual magnetic field. Numbers are the decimal part of the electron affinity, to be added to 16 752. Uncertainties, for their statistical part, are twice the standard deviations.

Linear regressions	$B_\perp = 0$	$B_\perp = 0.06\,\mu$T	$B_\perp = 0.12\,\mu$T
with no constraint	0.9760(27)	0.9762(27)	0.9765(27)
$K_0 = \langle K \rangle \,|\, \sigma_K = 0.6\%$	0.9763(18)	0.9765(18)	0.9773(18)
$K_0 = \langle K \rangle \,|\, \sigma_K = 0.3\%$	0.9764(12)	0.9767(12)	0.9777(12)

of the set of ${}^eA(\overline{\epsilon} = 0)$ obtained from the different series. As along one criterion or the other the dispersion appears to significantly increase above $B_\perp = 1.2 \times 10^{-7}$ T, no higher value of $B_\perp$ is considered.

A possible improvement of the method is to take into account the fact that the actual electric field intensity, hence the bias, depends on which electron spot is considered. The spots are actually separated by several millimeters as can be seen in Figure 2, which is quite the same order of magnitude as the supposed shift of their average position off axis. Correspondingly, the linear regression can be made a two-dimensional one, i.e. ${}^eA$ a linear function of ϵ and ϵ' with two coefficients K and K', respectively.

As a matter of fact, the obtained results appear significant only when the positions of the spots have been maintained really identical for the whole series, i.e. only in three instances. In these cases, the ${}^eA$ value is actually less biased by the photoelectron spot produced closer to the centre of the interaction chamber than by the one made further off-axis. The average of the three ${}^eA$ values so obtained assuming a zero magnetic field is ${}^eA = 16\,752.975\,4(43)$ cm^{-1}, which is compatible but less accurate than what can be found by the single-K fitting method (see Tab. 1). This method, though an interesting one for future experiments where the interaction zones are set at fixed places, will thus not contribute in a significant way to the determination of electron affinities with the present data.

The extreme possible values read from Table 1 are 16 752.9733 and 16 752.9792, which can be summarized as a 16 752.9762(30) overall result. Though one can hope that a part of the lambdameter error has been reduced by this averaging, one cannot exclude that the older lambdameter was bad enough to put an irreducible systematic constant error on the λ measurements, that the more modern WS8 device cannot completely wash out, for it was only used for the last 10% of the measurements. Since the two apparatuses were checked once to agree within 0.6 mk, 1 mk appears as a reasonable estimate of the maximum residual systematic error due to wavelength measurements. With the extra ± 0.7 mk uncertainty calculated in the introduction, the experimental result finally is ${}^eA(\mathrm{S}) = 16\,752.9762(47)\,cm^{-1}$. Taking the 1985 measurements [21] into account, one can propose $16\,752.974(5)\,cm^{-1}$ as the new recommended value of the electron affinity of ^{32}S. With the uncertainty on the conversion parameter [25] taken into account, this is 2.077 104 0(9) eV.

4 Silicon

The electron affinity of Silicon has already been measured by photodetachment microscopy [3], which improved the 11 207.24(15) cm^{-1} figure [26] to 11 207.252(18) cm^{-1}. However, re-examining the data confirms the trend for a well-defined variation of the measured electron affinity with the average photoelectron energy $\overline{\epsilon}$. Though this functional dependence is partly hidden by the dispersion of the individual measurements, as can be observed in Figure 4, extrapolation to zero electric field can provide a result made free of the electric field uncertainty.

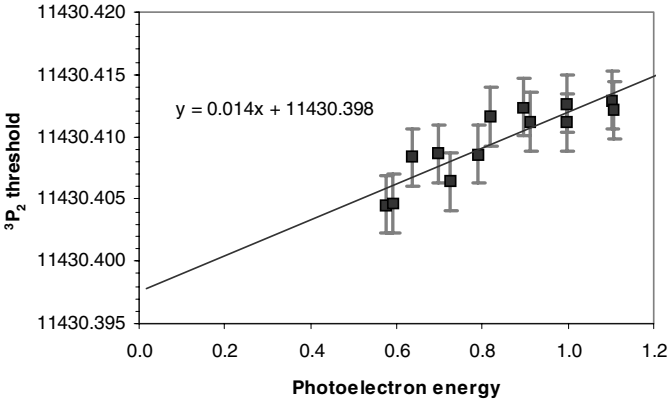

Fig. 4. Energy of the ${}^3P_2$ detachment threshold in Si^- as a function of the mean kinetic energy of the photoelectron (units are cm^{-1} for both), for a series of detachment experiments in an electric field $F \simeq 435$ V/m, assuming the presence of a magnetic field $B_\perp = 8 \times 10^{-8}$ T. The adjusted slope is $1.4 \pm 0.4\%$. The energy of the ${}^3P_2$ level, to be subtracted from the measured threshold to get the electron affinity, is 223.1572 cm^{-1}.

The fine-structure splittings of the ${}^3P$ ground term of silicon are so well-known [27,28] that detachment to the ${}^3P_0$, ${}^3P_1$, and ${}^3P_2$ thresholds produces equally useful measurements of the electron affinity, as long as one does not aim at an accuracy better than 0.1 mk. Seven series, such as the one presented in Figure 4, have been studied, which provide us with a total of 74 images. The average slope $\langle K \rangle$ coming from the linear regression of the ${}^eA$ values as a function of $\overline{\epsilon}$ is $1.0\% \pm 0.4\%$ with no magnetic-field correction, $1.2\% \pm 0.4\%$ at $B_\perp = 8 \times 10^{-8}$ T.

Table 2 shows the different possible statistical averages that can be obtained from the data. Two-dimensional linear fitting at $B_\perp = 0$ with a pair of coefficients K and K' gives $11\,207.2444(21)\,cm^{-1}$, which does not add

Table 2. Possible values for the electron affinity of silicon (cm^{-1}), depending on the deviation admitted for the energy bias and the assumed value of the residual magnetic field. Numbers are the decimal part of the electron affinity, to be added to 11 207. Uncertainties, for their statistical part, are twice the standard deviations.

Linear regressions	$B_\perp = 0$	$B_\perp = 0.06\,\mu$T	$B_\perp = 0.12\,\mu$T
with no constraint	0.2436(31)	0.2437(31)	0.2437(31)
$K_0 = \langle K \rangle \,|\, \sigma_K = 0.6\%$	0.2439(21)	0.2449(22)	0.2480(22)
$K_0 = \langle K \rangle \,|\, \sigma_K = 0.3\%$	0.2441(15)	0.2456(15)	0.2502(15)

anything to the information extracted from the one-K, $B_\perp = 0$ fittings. From the extreme values one gets a $11\,207.2461(55)\,cm^{-1}$ estimate. The uncertainty still has to be augmented by the already described possible systematic errors, which finally provides ${}^eA(\mathrm{Si}) = 11\,207.246(8)\,cm^{-1}$, i.e. 1.389 521 3(13) eV.

5 Oxygen

5.1 History of the electron affinity measurements of O

The history of the electron affinity of oxygen was recently summarized in several review articles [24,29]. The measurements made for the last 20 years are presented in Figure 5. The modern part of it began in 1985, when a laser photodetachment experiment produced a three-orders-of magnitude improvement on the electron affinity, down to a ±6 mk accuracy [30]. The Doppler effect, in this experiment, was eliminated by making the laser and ion beams co-propagating, then counter-propagating, and averaging the two extreme Doppler-shifted thresholds. In such a configuration, geometrical averaging directly corrects the Doppler effect at all orders [31]. Relying on the very numbers given in the original article, one could then obtain ${}^eA({}^{16}\mathrm{O}) = 11\,784.648(6)\,cm^{-1}$. But the threshold data of this experiment, published as illustrations in the 1985 review of electron affinities [32], would lead to a somewhat higher value, which made one of the authors of the review think later that $11\,784.675(6)\,cm^{-1}$ was the value that should have come out of the experiment [33].

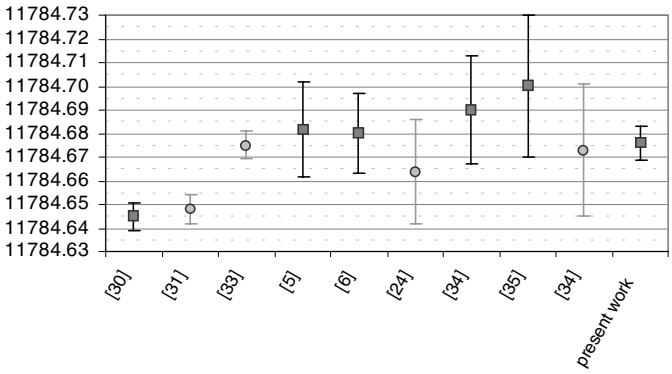

Fig. 5. The recent measurements of the electron affinity of ${}^{16}\mathrm{O}$, in chronological order. Black squares are the original measurements, grey circles are later revised or recommended values. Units are cm^{-1}.

The question actually arose when photodetachment microscopy measurements made around 2000 found a $11\,784.682(20)$, then a $11\,784.680(16)\,cm^{-1}$ value [5,6], which was incompatible with the 1985 measurement. This puzzling situation has been more clear since new independent measurements were made in 2002 and 2003, with a different technique [34,35]. These experiments agree with the more recent, not the 1985 measurement.

5.2 Results

The already described fitting methods have been applied to the data obtained by photodetachment of ${}^{16}\mathrm{O}^-$. These data comprise nine series recorded at different ion velocities and electric fields ranging from 101 to 536 Vm^{-1}. Figure 6 gives one of them as a typical example, which shows why assuming a linear variation of ${}^eA$ with $\overline{\epsilon}$ was not strikingly evident on these early recordings.

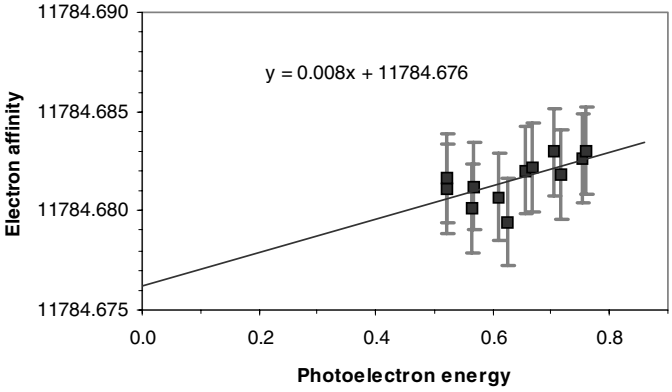

Fig. 6. Detachment threshold of O^- as a function of the mean kinetic energy of the photoelectron (units are cm^{-1}), for a series of detachment experiments in an electric field $F \simeq 250\,V/m$, assuming the presence of a magnetic field $B_\perp = 8 \times 10^{-8}\,T$. Weighted fitting produces a $0.8 \pm 0.7\,\%$ slope.

Table 3 gives the possible values for the electron affinity of ${}^{16}\mathrm{O}$. The slopes K obtained by free linear regressions are smaller than those obtained with Si and S, probably because in these older series, the experimental conditions were less constant than for the more recent ones, which washed the $\overline{\epsilon}$ dependence out. To take into account the possibility that a 1.5% error on the F value nevertheless exist, two additional lines are included, that give the average values of ${}^eA(\mathrm{O})$ obtained

Table 3. Possible values for the electron affinity of oxygen (cm^{-1}), depending on the deviation admitted for the energy bias and the assumed value of the residual magnetic field. Numbers are the decimal part of the electron affinity, to be added to 11 784. Uncertainties, for their statistical part, are twice the standard deviations.

Linear regressions	$B_\perp = 0$	$B_\perp = 0.06\,\mu$T	$B_\perp = 0.12\,\mu$T
with no constraint	0.6767(29)	0.6767(29)	0.6767(29)
$K_0 = \langle K \rangle \,|\, \sigma_K = 0.006$	0.6752(19)	0.6760(19)	0.6783(19)
$K_0 = \langle K \rangle \,|\, \sigma_K = 0.003$	0.6754(13)	0.6762(13)	0.6788(13)
$K_0 = 1\% \,|\, \sigma_K = 0.006$	0.6736(19)	0.6747(19)	0.6780(19)
$K_0 = 1\% \,|\, \sigma_K = 0.003$	0.6729(13)	0.6743(13)	0.6784(13)

constraining the linear regressions around a 1% slope. From the extreme possible values one gets an overall result ${}^eA(\mathrm{O}) = 11\,784.6759(43)\,\mathrm{cm}^{-1}$. With the additional systematic uncertainties, this is $11\,784.676(7)\,\mathrm{cm}^{-1}$, or 1.461 113 5(12) eV.

6 Conclusion

A thorough examination of the measurements performed with O^-, Si^- and S^- ions makes it possible to measure the error done when a pre-set value of the electric field was used. The unknown electric field error could thus be removed from the uncertainty budget of previous measurements. The three measured detachment energies are now the most well known of all electron affinities.

A straightforward improvement could be to record the next detachment microscopy images at strictly fixed positions of the ion-laser intersection, to eliminate the fluctuations due to variations in the electric field relative error. The interaction chamber could be redesigned too, to provide a larger volume with a nearly constant field.

Checking the statistical consistency of the numerical output for electron affinity values, we have set an upper limit to the residual magnetic field in the interaction region. Replacing the μ-metal magnetic shielding by active compensating coils could offer a better control of this field. Moreover it could open the way to new investigations of photodetachment dynamics in the presence of both magnetic and electric fields [7,22,36–40].

Appendix A: Linear regression with constrained slope

The maximum likelihood for a set of experimental kinetic energies ϵ_i and correspondingly measured affinities A_i with associated standard deviations σ_i, to sample a linear law $A = A_0 + K\epsilon$ with the constraint that K follows a normal distribution of probability around K_0 with a standard deviation σ_K, is reached for the (K, A_0) vector such that, if matrix $\mathbf{S}$ is defined as

$$\mathbf{S} = \begin{pmatrix} \sum_i \frac{\epsilon_i^2}{\sigma_i^2} + \frac{1}{\sigma_K^2} & \sum_i \frac{\epsilon_i}{\sigma_i^2} \\ \sum_i \frac{\epsilon_i}{\sigma_i^2} & \sum_i \frac{1}{\sigma_i^2} \end{pmatrix} \tag{A.1}$$

and vector $\mathbf{V}$ as

$$\mathbf{V} = \begin{pmatrix} \sum_i \frac{\epsilon_i A_i}{\sigma_i^2} + \frac{K_0}{\sigma_K^2} \\ \sum_i \frac{A_i}{\sigma_i^2} \end{pmatrix} \tag{A.2}$$

then

$$\begin{pmatrix} K \\ A_0 \end{pmatrix} = \mathbf{S}^{-1}\mathbf{V}. \tag{A.3}$$

The standard covariance matrix associated to the (K, A_0) result is exactly $\mathbf{S}^{-1}$. Its second diagonal element gives the variance σ_A^2 of the extrapolated electron affinity. Writing

$$\sigma_A^{-2} = \sum_i \frac{1}{\sigma_i^2} - \frac{\left(\sum_i \frac{\epsilon_i}{\sigma_i^2}\right)^2}{\sum_i \frac{\epsilon_i^2}{\sigma_i^2} + \frac{1}{\sigma_K^2}} \tag{A.4}$$

one easily checks that the tighter slope K is constrained, the more accurate A_0 will be, with a minimum variance which is just the ordinary variance of a weighted average

$$\lim_{\sigma_K \to 0} (\sigma_A^2) = \left[\sum_i \frac{1}{\sigma_i^2}\right]^{-1}.$$

On the other hand, supposing no constraint on the K coefficient is equivalent to making σ_K infinite, and reduces the above to ordinary formulae for linear regression.

References

1. Yu.N. Demkov, V.D. Kondratovich, V.N. Ostrovskii, Pis'ma Zh. Eksp. Teor. Fiz. **34**, 425 (1981); [JETP Lett. **34**, 403 (1981)]
2. C. Blondel, C. Delsart, F. Dulieu, Phys. Rev. Lett. **77**, 3755 (1996)
3. C. Blondel, C. Delsart, F. Goldfarb, J. Phys. B **34**, L281 and 2757 (2001)
4. C. Bracher, W. Becker, S.A. Gurvitz, M. Kleber, M.S. Marinov, Am. J. Phys. **66**, 38 (1998)
5. C. Valli, C. Blondel, C. Delsart, Phys. Rev. A **59**, 3809 (1999)
6. C. Blondel, C. Delsart, C. Valli, S. Yiou, M. Godefroid, S. Van Eck, Phys. Rev. A **64**, 052504 (2001)
7. T. Kramer, C. Bracher, M. Kleber, Europhys. Lett. **56**, 471 (2001)

8. D.A. Dahl, J.E. Delmore, A.D. Appelhans, Rev. Sci. Instrum. **61**, 607 (1990)
9. P. Juncar, J. Pinard, Opt. Commun. **14**, 438 (1975)
10. J.L. Hall, S.A. Lee, Appl. Phys. Lett. **29**, 367 (1976)
11. J. Cachenaut, C. Man, P. Cerez, A. Brillet, F. Stoeckel, A. Jourdan, F. Hartmann, Rev. Phys. Appl. **14**, 685 (1979)
12. Model 3391 of Quantar Technology Inc., 2620A Mission Street, Santa Cruz, CA 95060-5703
13. M.C. Baruch, W.G. Sturrus, N.D. Gibson, D.J. Larson, Phys. Rev. A **45**, 2825 (1992)
14. N.D. Gibson, B.J. Davies, D.J. Larson, Phys. Rev. A **48**, 310 (1993)
15. N. D. Gibson, M.D. Gasda, K.A. Moore, D.A. Zawistowski, C.W. Walter, Phys. Rev. A **64**, 061403 (2001)
16. I. I. Fabrikant, J. Phys. B: At. Mol. Opt. Phys. **27**, 4545 (1994)
17. R. Trainham, R.M. Jopson, D.J. Larson, Phys. Rev. A **39**, 3223 (1989)
18. N.B. Mansour, G.D. Fletcher, D.J. Larson, Phys. Rev. A **35**, 2321 (1987)
19. W.A.M. Blumberg, R.M. Jopson, D.J. Larson, Phys. Rev. Lett. **40**, 1320 (1978)
20. W.A.M. Blumberg, W.M. Itano, D.J. Larson, Phys. Rev. **19**, 139 (1979)
21. D.J. Larson, R. Stoneman, Phys. Rev. A **31**, 2210 (1985)
22. J.N. Yukich, T. Kramer, C. Bracher, Phys. Rev. A **68**, 033412 (2003)
23. W.C. Lineberger, B.W. Woodward, Phys. Rev. Lett. **25**, 424 (1970)
24. T. Andersen, H.K. Haugen, H. Hotop, J. Phys. Chem. Ref. Data **28**, 1511 (1999)
25. P.J. Mohr, B.N. Taylor, Rev. Mod. Phys. **77**, 1 (2005)
26. M. Scheer, R.C. Bilodeau, C.A. Brodie, H.K. Haugen, Phys. Rev. A **58**, 2844 (1998)
27. M. Inguscio, K.M. Evenson, V. Beltran-Lopez, E. Ley-Koo, Astrophys. J. **278**, L127 (1984)
28. J.M. Brown, L.R. Zink, K.M. Evenson, Astrophys. J. **423**, L151 (1994)
29. T. Andersen, Phys. Rep. **394**, 157 (2004)
30. D.M. Neumark, K.R. Lykke, T. Andersen, W.C. Lineberger, Phys. Rev. A **32**, 1890 (1985)
31. C. Blondel, Phys. Scripta T **58**, 31 (1995)
32. H. Hotop, W.C. Lineberger, J. Phys. Chem. Ref. Data **14**, 731 (1985)
33. H. Hotop, private communication, 1999
34. D.M. Pendergrast, J.N. Yukich, Phys. Rev. A **67**, 062721 (2003)
35. A.K. Langworthy, D.M. Pendergrast, J.N. Yukich, Phys. Rev. A **69**, 025401 (2004)
36. A.D. Peters, J.B. Delos, Phys. Rev. A **47**, 3020 (1993)
37. A.D. Peters, J.B. Delos, Phys. Rev. A **47**, 3036 (1993)
38. A.D. Peters, C. Jaffé, J.B. Delos, Phys. Rev. A **56**, 331 (1997)
39. A.D. Peters, C. Jaffé, J. Gao, J.B. Delos, Phys. Rev. A **56**, 345 (1997)
40. T. Kramer, C. Bracher, M. Kleber, J. Opt. B: Quant. Semiclass. Opt. **6**, 21 (2004)